(Preprint) AAS 25-320

EXTENDING EARTH–MOON TRANSFER BASED ON LOBE DYNAMICS INTO THE RESTRICTED FOUR-BODY PROBLEM

Naoki Hiraiwa[*], Mai Bando[†], and Shinji Hokamoto[†]

Recently the exploration of the Moon has been gaining attention again. This study aims to construct fuel-efficient transfer from the Earth to the Moon based on lobe dynamics. Lobe dynamics in the circular restricted three-body problem (CR3BP) typically indicates transport structures enclosed by the stable and unstable manifolds of resonant orbits. These structures help understand chaotic motions for trajectory design. By connecting chaotic trajectories based on lobe dynamics, the proposed method can find fuel-efficient low-energy transfers from the low Earth orbit to the low lunar orbit. The optimal transfer in the CR3BP is then converted into transfers in the bicircular restricted four-body problem (BCR4BP). The optimal transfer obtained in the BCR4BP is analyzed based on Lagrangian coherent structures and compared with other optimal transfers known in literature.

INTRODUCTION

In trajectory design, geometrical methods, the ones utilizing dynamical systems theory to save fuel consumption (e.g., References 1–8), contribute to the design of low-energy transfers by leveraging natural dynamics. The stable and unstable manifolds of periodic orbits typically identify dynamical structures, and these dynamical structures provide fuel-free pathways in the system. These fuel-free pathways contribute to building low-energy transfers. Geometrical methods can also generate good initial guesses to execute further numerical optimization.

One of the dynamical structures in spacecraft dynamics is tube dynamics.[1] Tube dynamics typically leverages the stable and unstable manifolds of libration point orbits to design transfers between primaries. These manifolds are called *tube*s because they have a cylindrical geometry. Another dynamical structure is lobe dynamics.[9] In the circular restricted three-body problem (CR3BP), the stable and unstable manifolds of resonant orbits help to identify lobe dynamics in the periapse Poincaré map. In this map, one can observe the transport by lobe dynamics in the chaotic zones around stable resonant tori. Previous work[7] proposes a trajectory design method to construct low-energy transfers by combining chaotic trajectories based on lobe dynamics. Compared to others,[10,11] this method can generate chaotic transfers with more feasible transfer time. However, the previous work[7] does not include the application to the trajectory design for a realistic mission scenario. Therefore, this paper aims to apply lobe dynamics to construct the optimal Earth–Moon transfer in the CR3BP. Specifically, the transfer from the low Earth orbit (LEO) with an altitude of 167 [km] to the low lunar orbit (LLO) with an altitude of 100 [km] is considered. The obtained optimal solution is then utilized to find the optimal Earth–Moon transfer in the bicircular restricted four-body problem

[*]Ph.D. student, Department of Aeronautics and Astronautics, Kyushu University, 819-0395, Japan.
[†]Professor, Department of Aeronautics and Astronautics, Kyushu University, 819-0395, Japan.

(BCR4BP). The transfer structure to the Moon in the optimal transfer in the BCR4BP is analyzed, and its fuel consumption and time of flight are compared to those in literature[12–20] to demonstrate the effectiveness of the proposed method.

OVERVIEW OF LOBE DYNAMICS

This section provides an overview of lobe dynamics especially in the CR3BP. Leveraging lobe dynamics is an essential part of the proposed method. At first, this idea was invented for the analysis of fluid mixing,[21] and then conceptualized as a dynamical structure in a general two-dimensional area-preserving map.[9] Here, the fundamental points related to lobe dynamics are summarized based on Reference.[7]

Circular Restricted Three-Body Problem (CR3BP)

This study construct a trajectory design method mainly in the CR3BP, whose coordinates are shown in Figure 1. This dynamical model considers the motion of a particle P_3 with small mass (spacecraft) under the gravitational forces from two celestial bodies P_1 and P_2. Therefore, $m_1 > m_2 \gg m_3$ is assumed when the masses of P_1, P_2, and P_3 are denoted as m_1, m_2, and m_3, respectively. In addition, it is assumed that P_1 and P_2 are in circular orbits around the barycenter of the system. The non-dimensional equations of motion of P_3 are then expressed as follows:

$$\begin{cases} \ddot{x} - 2\dot{y} = \dfrac{\partial U}{\partial x} \\ \ddot{y} + 2\dot{x} = \dfrac{\partial U}{\partial y} \\ \ddot{z} = \dfrac{\partial U}{\partial z} \end{cases}, \tag{1}$$

where the position of P_3 is $[x,\ y,\ z]^{\mathrm{T}}$ and U is the pseudo-potential function given by

$$U = \frac{1}{2}\left(x^2 + y^2\right) + \frac{1-\mu}{r_1} + \frac{\mu}{r_2} + \frac{1}{2}\mu\left(1-\mu\right), \tag{2}$$

$$r_1 = \sqrt{(x+\mu)^2 + y^2 + z^2}, \tag{3}$$

$$r_2 = \sqrt{\{x-(1-\mu)\}^2 + y^2 + z^2}. \tag{4}$$

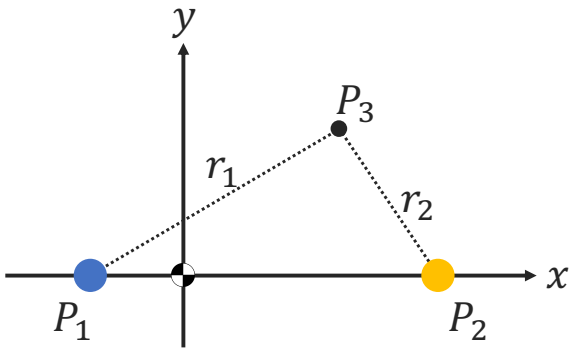

Figure 1: Coordinates in the CR3BP

The non-dimensional mass ratio μ is defined as $\mu = m_2/(m_1 + m_2)$. In the Earth–Moon system, μ is set to be 1.21509×10^{-2}. The CR3BP has one integral of motion called the Jacobi constant C_J defined as:

$$C_J = 2U - \left(\dot{x}^2 + \dot{y}^2 + \dot{z}^2\right). \tag{5}$$

In this study, the Jacobi constant is set to be $C_J = 3.16$.

Periapse Poincaré Map

When the Jacobi constant is fixed ($C_J = 3.16$ in this study), the dynamics in the planar CR3BP can be represented by a two-dimensional Poincaré map. The periapse Poincaré map is a Poincaré map whose surface of section lies in periapsis passage. In the planar CR3BP, the periapse Poincaré map is utilized to detect lobe dynamics by observing the stable and unstable manifolds of resonant orbits. Since lobe dynamics is defined in a area-preserving map, this map is expressed by using Delaunay elements.[22]

The state of P_3 in the planar CR3BP, $(x,\ y,\ \dot{x},\ \dot{y})$, is transformed into the Delaunay elements $(l_d,\ g_d,\ L_d,\ G_d)$. First, the state in the rotating frame is converted into that in a temporary inertial frame, $(X,\ Y,\ \dot{X},\ \dot{Y})$, as follows:

$$\begin{bmatrix} X \\ Y \\ \dot{X} \\ \dot{Y} \end{bmatrix} = \begin{bmatrix} 1 & 0 & 0 & 0 \\ 0 & 1 & 0 & 0 \\ 0 & -1 & 1 & 0 \\ 1 & 0 & 0 & 1 \end{bmatrix} \begin{bmatrix} x+\mu \\ y \\ \dot{x} \\ \dot{y} \end{bmatrix} \tag{6}$$

In this inertial frame, the classical orbital elements, the semi-major axis a, eccentricity e, argument of periapsis ω, and true anomaly f, are defined such that

$$a = \frac{(1-\mu)\, r_1}{2\,(1-\mu) - r_1 V^2}, \tag{7}$$

$$\boldsymbol{e} = -\frac{(\boldsymbol{r}_1 \times \boldsymbol{V}) \times \boldsymbol{V}}{1-\mu} - \frac{\boldsymbol{r}_1}{r_1}, \qquad e = \|\boldsymbol{e}\|, \tag{8}$$

ω is the angle from the X-axis to the $\boldsymbol{e}$ vector, and f is the angle from the $\boldsymbol{e}$ vector to the $\boldsymbol{r}_1$ vector, where

$$\boldsymbol{r}_1 = \begin{bmatrix} X \\ Y \\ 0 \end{bmatrix}, \qquad r_1 = \|\boldsymbol{r}_1\|, \qquad \boldsymbol{V} = \begin{bmatrix} \dot{X} \\ \dot{Y} \\ 0 \end{bmatrix}, \qquad V = \|\boldsymbol{V}\|. \tag{9}$$

Note that the inclination is zero, and the angular momentum in the inertial frame, $X\dot{Y} - Y\dot{X}$, is assumed to be positive in this map. Finally, the Delaunay elements are calculated from the classical orbital elements as follows:

$$l_d = M = E - e\sin E, \tag{10}$$

$$g_d = \omega, \tag{11}$$

$$L_d = \sqrt{(1-\mu)\, a}, \tag{12}$$

$$G_d = \sqrt{(1-\mu)\, a\, (1-e^2)}, \tag{13}$$

where M is the mean anomaly, E is the eccentric anomaly defined by

$$E = 2\tan^{-1}\left(\sqrt{\frac{1-e}{1+e}}\tan\frac{f}{2}\right). \tag{14}$$

Note that G_d means the magnitude of the angular momentum $h = |X\dot{Y} - Y\dot{X}|$ in the inertial frame. Periapsis passage is defined as $f = 0$, and this condition is equivalent to $l_d = 0$ in the Delaunay elements.

Lobe sequence and effective lobe

Practically, a *lobe* is a region enclosed by the stable and unstable manifolds of resonant orbits in the periapse Poincaré map. Lobe dynamics explains the transport between lobes, and a series of this transport is called a *lobe sequence*.[7] For trajectory design, it is important to focus on lobes that help to construct robust transfers. When a radius of a lobe is defined as the radius of the largest circle within the lobe, an *effective lobe*[7] is defined as a lobe whose radius is larger than a threshold r^*. In this study, r^* is set to be 0.002, and Figure 2 shows an example of a lobe sequence enclosed by the stable and unstable manifolds associated with the 3:1 unstable resonant orbit. The number in the figure indicates the order of transfer.

Lobes related to the 3:1 and 7:2 unstable resonant orbits are utilized to construct Earth–Moon transfers in this study. Figure 3 demonstrates all the effective lobe sequences leveraged for trajectory

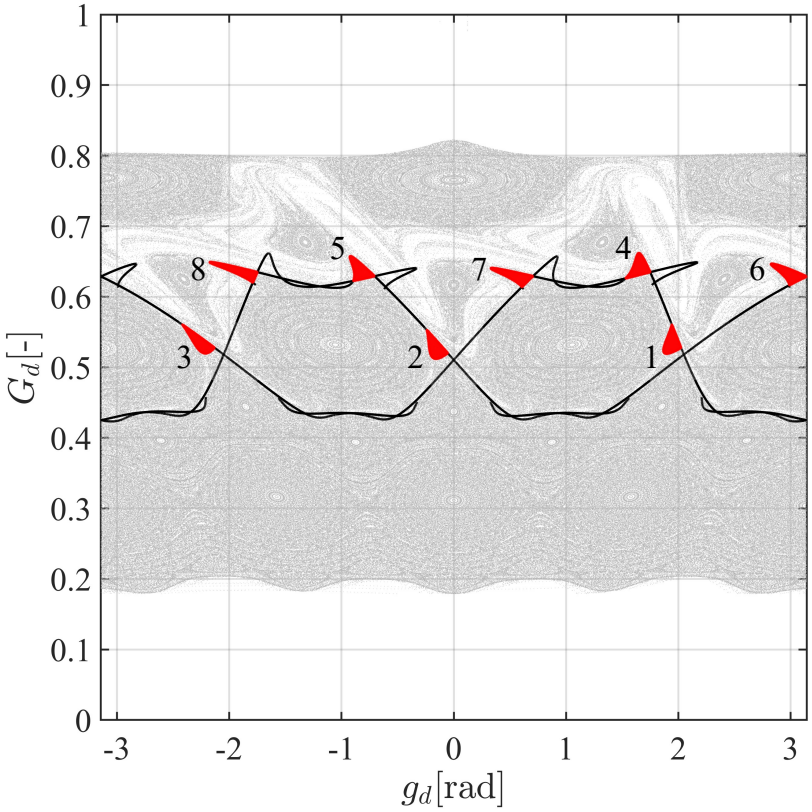

Figure 2: Example of a lobe sequence related to the 3:1 unstable resonant orbit

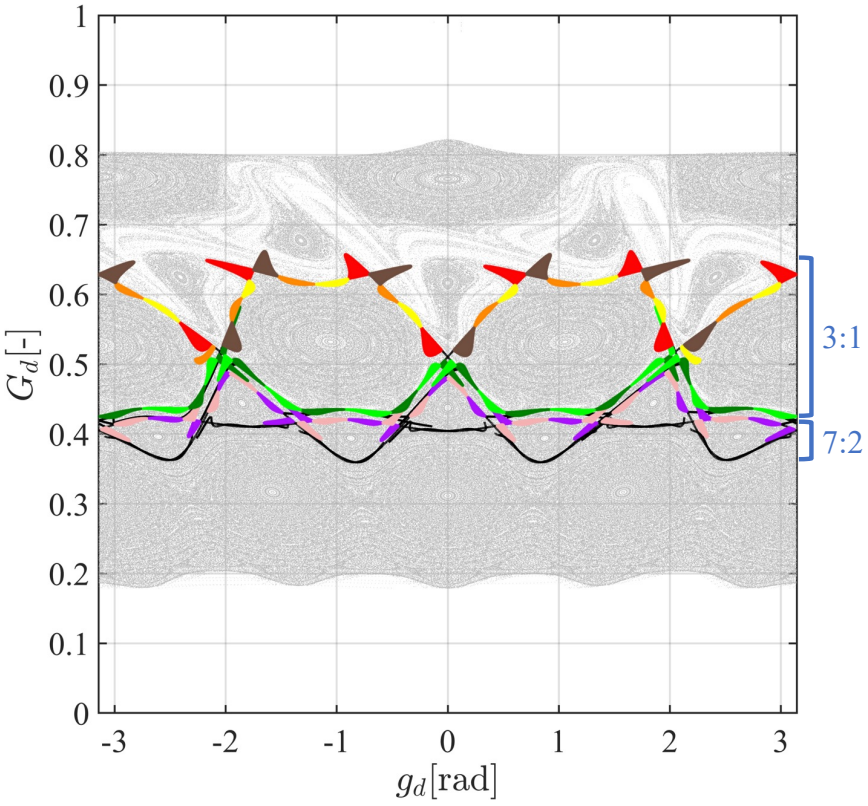

Figure 3: Effective lobe sequences for the Earth–Moon transfer design in the CR3BP

design in the CR3BP. Different sequences are shown in different colors. The transfer within the same sequence is based on natural dynamics, but control inputs are necessary to transfer between different sequences within a reasonable transfer time.

TRAJECTORY DESIGN IN THE CR3BP

This section describes the proposed method to design transfers from the LEO, the circular orbit around the Earth with an altitude of 167 [km], to the LLO, the circular orbit around the Moon with an altitude of 100 [km], based on effective lobe sequences in the CR3BP. The altitude of LEO and LLO is determined from the literature[12–20] to compare the results in the next section. The framework of the trajectory design is the same to that in the previous work,[7] but in this study the departure and arrival orbits have Jacobi constants different from intermediate transfer arcs within effective lobe sequences with $C_J = 3.16$.

Transfer Design Based on the Graph Structure

Under some assumptions, the potential pathways between the LEO and LLO are represented by a graph structure. The LEO and LLO are discretized equally into 12 points, and effective lobes in Figure 3 are represented by their centroids. The first ΔV is applied to depart from one of the LEO points and move into a trajectory with $C_J = 3.16$, and the direction of this ΔV is along the velocity direction. Subsequently, the spacecraft is inserted into one of the effective lobe sequences with the next ΔV. Other ΔVs are applied to move between the lobe sequences. The ΔV for the transfer

between trajectories with the same $C_J = 3.16$ is calculated based on Figure 4. The ΔVs are added at the crossing point in the x-y plane to change only the velocity direction. This process is repeated until the spacecraft reaches ballistic transfer trajectories to the LLO. Finally, the last ΔV is applied to circularize the transfer trajectory at one of the LLO points. To efficiently search for the optimal transfer, the order of transfers is designed so that G_d increases monotonically, as shown in Figure 5. In this figure, the color of each box corresponds to the color of the effective lobe sequences in Figure 3. Specifically, the spacecraft first moves from the LEO to the purple or pink lobe sequence, and then waits for the next ΔV in the same sequence. The spacecraft moves into the other sequences and executes several ΔVs until it reaches the LLO. In addition, the routes whose ΔV is less than 400 [m/s] are considered to reduce the number of potential transfer routes. The fuel-optimal transfer can be found by calculating the total ΔV for all the potential transfers under the above assumptions.

Results in the CR3BP

Based on the graph representing the structure in Figure 5, the optimal Earth–Moon transfer is found as shown in Figure 6. Blue arrows in the figure indicate the ΔVs at each point, and the length of the arrows corresponds to the relative magnitude of the ΔVs. The first ΔV at the triangular point on the LEO delivers the spacecraft to the black trajectory with $C_J = 3.16$. Then, the spacecraft is inserted into the purple, yellow green, and red lobe sequences in this order. The last ΔV at the star point on the LLO circularizes the transfer trajectory. As a result, the total ΔV is 4275 [m/s], and the time of flight is 192 [day]. The four large ΔVs contribute to the majority of the total ΔV, but

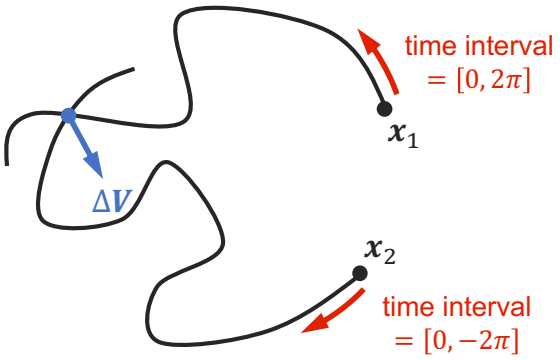

Figure 4: Illustration of the way of building an impulsive transfer.

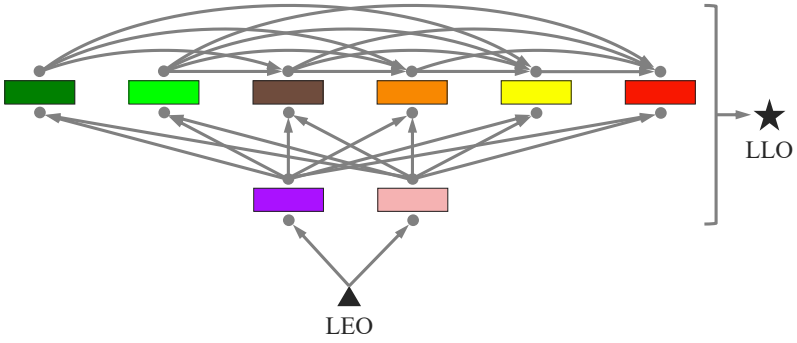

Figure 5: The order of transfers

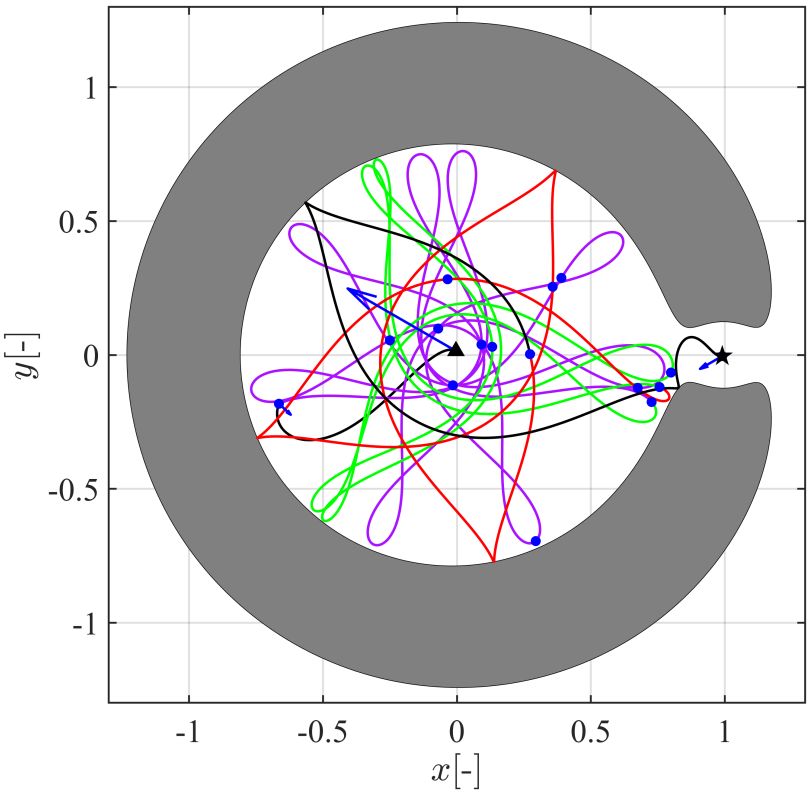

Figure 6: Optimal transfer in the CR3BP

the other ΔVs are necessary to adjust the trajectory under the chaotic dynamics.

TRAJECTORY DESIGN IN THE BCR4BP

The optimal transfer in the CR3BP (Figure 6) is utilized as the initial guess to solve the optimization of the Earth–Moon transfer in the BCR4BP. This transfer trajectory is constructed based on lobe dynamics in the Earth–Moon CR3BP, so it is useful to investigate this initial guess can contribute to designing fuel-efficient transfers in the BCR4BP.

Bicircular Restricted Four-Body Problem (BCR4BP)

The BCR4BP can be regarded as a dynamical model of the Earth–Moon system with the perturbation of the Sun S, and its coordinates are shown in Figure 7. The Sun is assumed to rotate around the barycenter of the Earth–Moon system with a circular orbit. The non-dimensional mass of the Sun, m_s, is set to be 3.28914×10^5, and the non-dimensional distance between the Sun and the barycenter of the Earth–Moon system, a_s, is set to be 3.89173×10^2. When the phase angle of the Sun is denoted by θ_s, this angle satisfies

$$\theta_s = \theta_s^* + \omega_s t, \tag{15}$$

where θ_s^* is the initial phase angle of the Sun, and ω_s is the non-dimensional angular velocity of the Sun. Subsequently, the position of the Sun, $(x_s,\ y_s,\ z_s)$, is expressed as

$$x_s = a_s \cos\theta_s, \qquad y_s = a_s \sin\theta_s, \qquad z_s = 0. \tag{16}$$

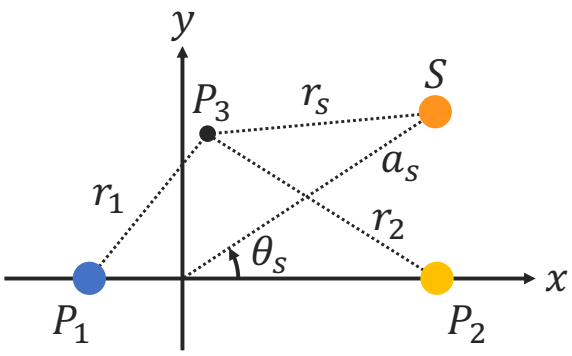

Figure 7: Coordinates in the BCR4BP

The non-dimensional equations of motion of P_3 are expressed as follows:

$$\begin{cases} \ddot{x} - 2\dot{y} = \dfrac{\partial \Upsilon}{\partial x} \\ \ddot{y} + 2\dot{x} = \dfrac{\partial \Upsilon}{\partial y} \\ \ddot{z} = \dfrac{\partial \Upsilon}{\partial z} \end{cases}, \tag{17}$$

where

$$\Upsilon = \frac{1}{2}\left(x^2 + y^2\right) + \frac{1-\mu}{r_1} + \frac{\mu}{r_2} + \frac{m_s}{r_s} - \frac{m_s}{a_s^3}\left(x_s x + y_s y + z_s z\right), \tag{18}$$

$$r_s = \sqrt{(x - x_s)^2 + (y - y_s)^2 + (z - z_s)^2}. \tag{19}$$

Transfer Design in the BCR4BP

Since the BCR4BP is a non-autonomous system, the initial phase angle of the Sun, θ_s^*, is discretized as $\theta_s^* = k\pi/6$ $(k = 0, 1, \cdots, 11)$ to construct the initial guesses in the BCR4BP from the trajectory in Figure 6. This trajectory in Figure 6 is constructed by propagating the centroid of the lobes forward and backward in time as illustrated in Figure 8. The color of segments in Figure 8 corresponds to the color of the trajectories in Figure 6. Each segment is divided so that the transfer time of each segment satisfies $\Delta t \simeq 1$. As a result, the number of segments becomes $N = 45$. The initial points of each divided segment are propagated by Eq. (17) to construct the initial guesses for the optimization. The optimization problem is formulated as follows:

$$\text{minimize} \qquad \Delta V_{\mathrm{E}} + \sum_{n=1}^{N-1} \left\| \boldsymbol{v}_{n+1}^{i} - \boldsymbol{v}_{n}^{f} \right\| + \Delta V_{\mathrm{M}} \tag{20}$$

$$\text{subject to} \qquad \boldsymbol{r}_1^i = \boldsymbol{r}_{\mathrm{E}} \tag{21}$$

$$\theta_{s,1}^i = \theta_s^* \tag{22}$$

$$\boldsymbol{r}_{n+1}^i = \boldsymbol{r}_n^f \ (n = 1, 2, \cdots, N-1) \tag{23}$$

$$\theta_{s,n+1}^i = \theta_{s,n}^f \ (n = 1, 2, \cdots, N-1) \tag{24}$$

$$\boldsymbol{r}_N^f = \boldsymbol{r}_{\mathrm{M}} \tag{25}$$

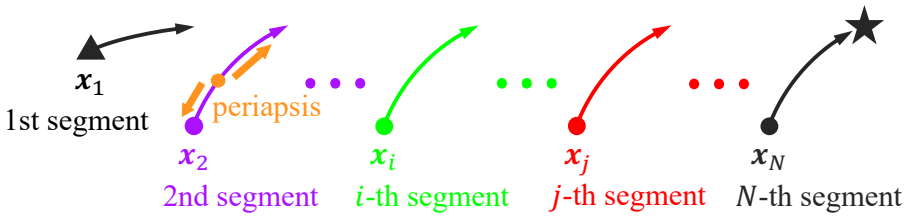

Figure 8: Illustration of the segments that construct the trajectory in Figure 6

where the state along the n-th segment is denoted by $\boldsymbol{x}_n$ ($n = 1, 2, \cdots, N$). The position, velocity, and phase angle of the Sun within $\boldsymbol{x}_n$ are represented by $\boldsymbol{r}_n$, $\boldsymbol{v}_n$, and $\theta_{s,n}$, respectively. The initial and final points of the segments are expressed by $(\cdot)^i$ and $(\cdot)^f$, respectively. The ΔV_{E} is the ΔV to depart from the LEO, and the ΔV_{M} is the ΔV to circularize the transfer trajectory at the LLO. These ΔVs can be executed in any direction. The starting position at the LEO is $\boldsymbol{r}_{\mathrm{E}}$, and the final position at the LLO is $\boldsymbol{r}_{\mathrm{M}}$. These positions $\boldsymbol{r}_{\mathrm{E}}$ and $\boldsymbol{r}_{\mathrm{M}}$ are the same as those in Figure 6. This optimization problem is solved by the *fmincon* function in MATLAB with SQP algorithm.

The results of the optimization in the BCR4BP are summarized in Table 1. The "-" in the table indicates that the optimization for the corresponding θ_s^* does not converge after 50000 iterations. All the converged solutions have the time of flight similar to that of the initial guess (193 [day]), but the total ΔV changes drastically. Therefore, the best solution in the table is the one with $\theta_s^* = 0$. Figure 9 demonstrates the optimal transfer in the BCR4BP with $\theta_s^* = 0$. The dashed line in the figure indicates the optimal trajectory in the CR3BP (Figure 6), and the solid line represents the optimal trajectory in the BCR4BP. The triangular and star points in the figure correspond to the points on the LEO and LLO, respectively. Similar to Figure 6, the blue arrows indicate the ΔVs at each point, and the length of the arrows corresponds to the relative magnitude of the ΔVs. In this case, the optimal trajectory is similar to two-impulsive transfers, although small other ΔVs are necessary to adjust the transfer trajectory.

Table 1: Results of the optimization in the BCR4BP

θ_s^*	Total ΔV [m/s]	Time of Flight [day]
0	3833	193
$\pi/6$	-	-
$\pi/3$	-	-
$\pi/2$	5201	192
$2\pi/3$	3842	194
$5\pi/6$	-	-
π	-	-
$7\pi/6$	-	-
$4\pi/3$	-	-
$3\pi/2$	4935	193
$5\pi/3$	3848	194
$11\pi/6$	3838	193

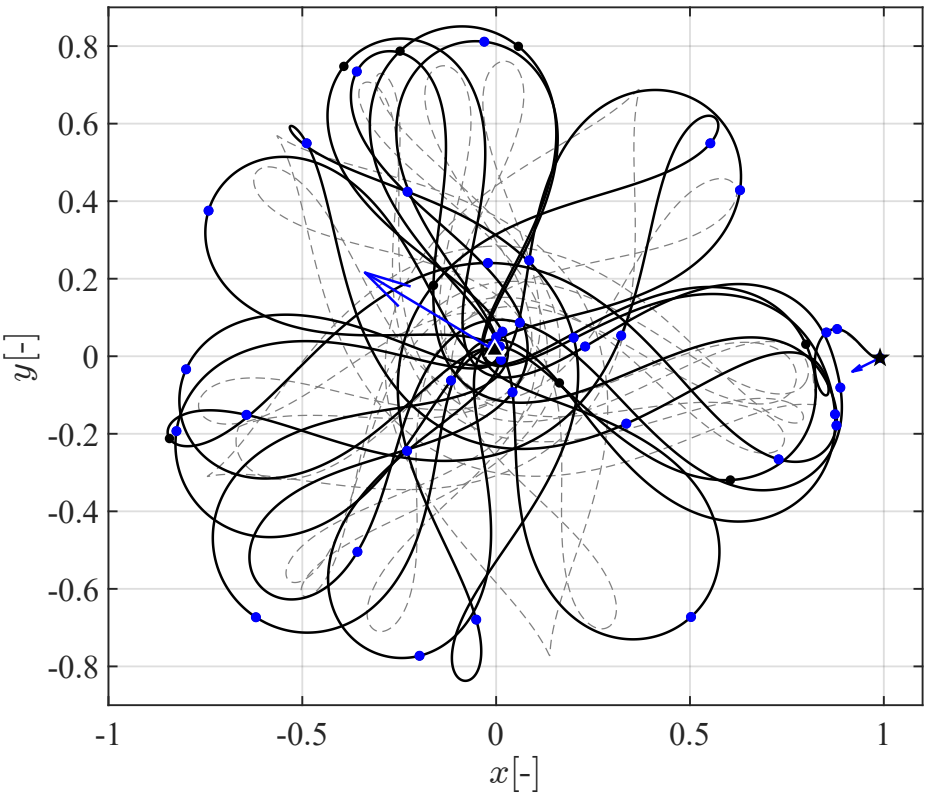

Figure 9: Optimal transfer in the BCR4BP

ANALYSIS OF THE OBTAINED RESULTS IN THE BCR4BP

This section analyzes the optimal Earth–Moon transfer in the BCR4BP (Figure 9) based on the Lagrangian coherent structures (LCSs)[23–25] and compare its fuel consumption and time of flight with those in the literature.[12–20]

Analysis of the Optimal Transfer in the BCR4BP

The transfer structure to the Moon along the optimal trajectory of Figure 9 is analyzed. The Jacobi constant in the Earth–Moon CR3BP, perturbed by the gravitational force of the Sun, is calculated along this optimal trajectory, as shown in Figure 10. The cyan region in Figure 10(b) has the perturbed Jacobi constant $C_J \simeq 3.16$ (precisely, $3.1551 < C_J < 3.1666$). The corresponding optimal trajectory is also plotted as the cyan region in Figure 10(a). This result implies that the transfer structure to the Moon in the CR3BP with $C_J = 3.16$, i.e., the stable manifold of the L_1 Lyapunov orbit, may remain in the BCR4BP. However, analyzing the dynamical structures in the BCR4BP is difficult because the perturbation of the Sun alters the dynamical system into a non-autonomous one.

For the analysis of transfer structures in the non-autonomous system of the BCR4BP, LCSs are utilized in this study. Haller[24] has given a definition of LCSs as local extrema of the finite-time Lyapunov exponent (FTLE). The FTLE at $\boldsymbol{x}$ from $t = 0$ to $t = T$ is defined as

$$\sigma(\boldsymbol{x}, T) = \frac{1}{|T|} \ln \|\Phi(T, 0)\| \tag{26}$$

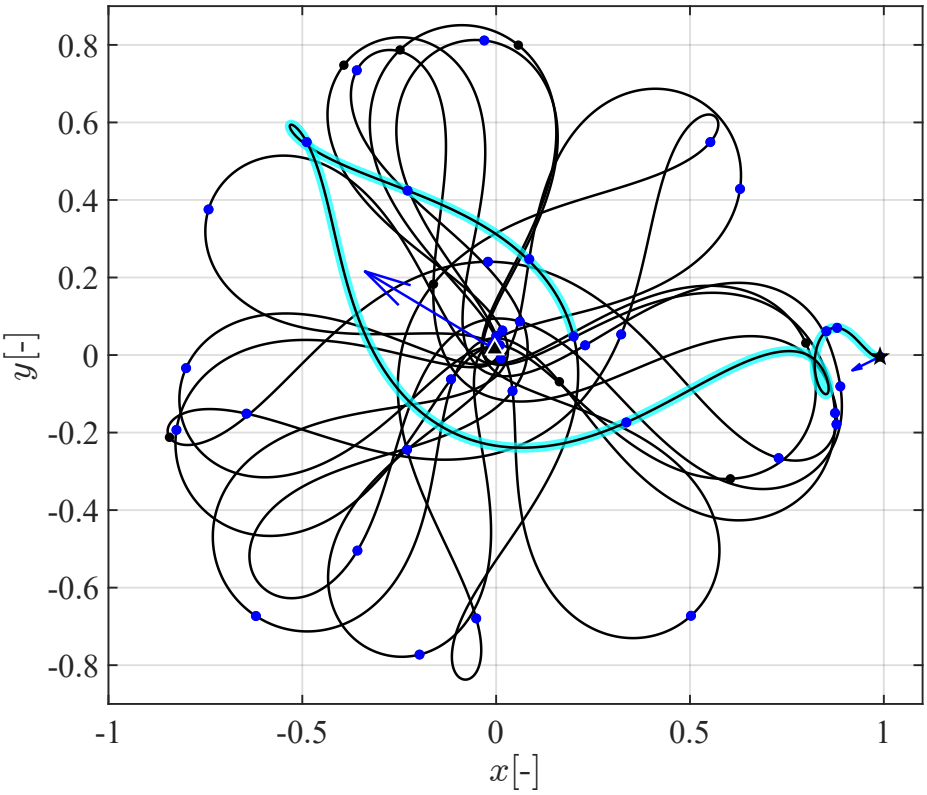

(a) Optimal trajectory with the perturbed Jacobi constant $C_J \simeq 3.16$

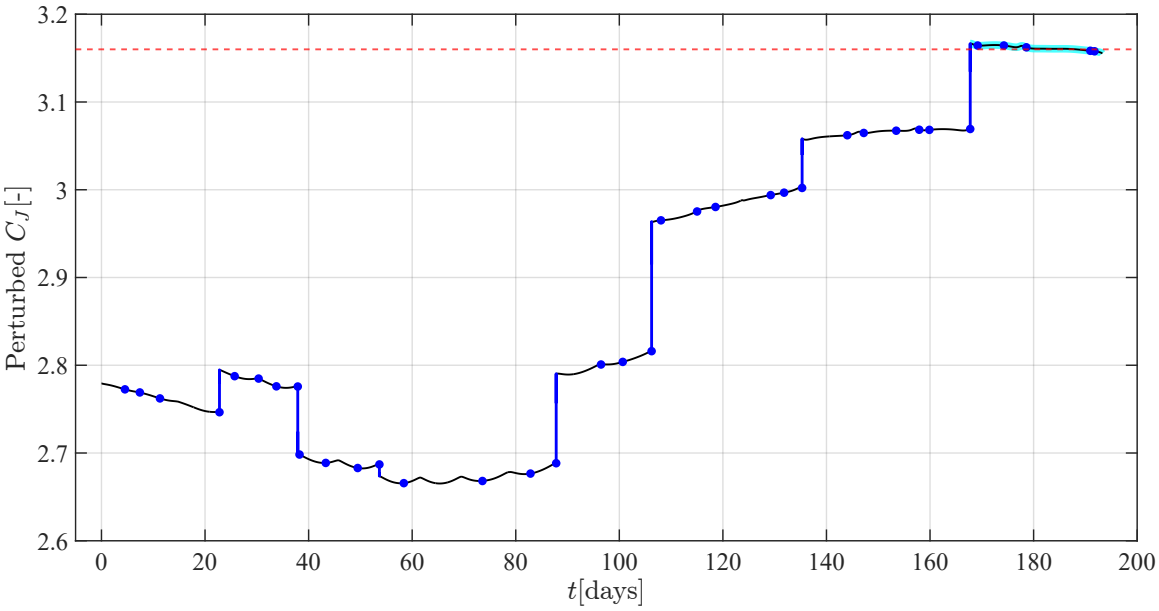

(b) Perturbed Jacobi constant in the Earth–Moon CR3BP

Figure 10: Perturbed Jacobi constant in the Earth–Moon CR3BP along the optimal trajectory in the BCR4BP

where $\Phi(T,0)$ is the state transiton matrix from $t = 0$ to $t = T$ along the reference trajectory starting from $\boldsymbol{x}$, and $\|\Phi(T,0)\|$ denotes the square root of the largest eigenvalue of the Cauchy–Green strain tensor $\Phi(T,0)^{\mathrm{T}}\Phi(T,0)$. In autonomous systems, LCSs correspond to the stable and unstable manifolds associated with invariant tori. On the other hand, in non-autonomous systems, LCSs can represent manifold-like lines or surfaces that mediate the phase space transport.

Literature of astrodynamics demonstrated that LCSs can be detected based on the FTLE in the CR3BP[26,27] and in the elliptic restricted three-body problem.[28] Reference 29 investigated LCSs in the CR3BP, BCR4BP, and the Sun–Earth–Moon ephemeris model by analyzing the FTLE fields. In practice, LCSs are detected by evaluating the FTLE value of grided points at a surface of section. Similar to Reference 29, the FTLE field at the surface of section of $x = 0.8$ is examined under the dynamics of the BCR4BP. Figure 11 shows the stable and unstable manifolds of the L_1 Lyapunov orbit at $x = 0.8$ as a reference of the LCS in the CR3BP. For the calculation of FTLE fields, a grid of 1000×1000 points is set within the region of $-0.1658 \leq y \leq 0.1658$ and $-0.2325 \leq \dot{y} \leq 0.2325$. The forward-time FTLE fields in the CR3BP and BCR4BP (with $\theta_s^* = 297.1825$ [deg]) are calculated with $T = 14$ [day], as shown in Figure 12. With this time interval, the ridges in the FTLE field in the CR3BP match the stable manifold of the L_1 Lyapunov orbit, as shown in Figure 12(b). In this figure, dotted line denotes this stable manifold. Figure 12(c) indicate the FTLE field in the BCR4BP, and the difference of the FTLE fields in the CR3BP and BCR4BP is shown in Figure 12(d). The blue and red lines in Figure 12(d) reveals that the ridges in the FTLE fields changes slightly due to the perturbation of the Sun. The cross in Figure 12(c) represent the cyan region of Figure 9 at $x = 0.8$ along the optimal trajectory, and the phase angle of the Sun is $\theta_s = 297.1825$ [deg] at this point. Figure 12(c) reveals that the obtained optimal trajectory is located slightly inside the ridges of the FTLE field in the BCR4BP. Thus, the obtained optimal trajectory passes through the region divided by the LCS in the BCR4BP to transfer to the Moon, and this LCS in the BCR4BP can be understood as the perturbed stable manifold of the L_1 Lyapunov orbit with $C_J = 3.16$ in the CR3BP.

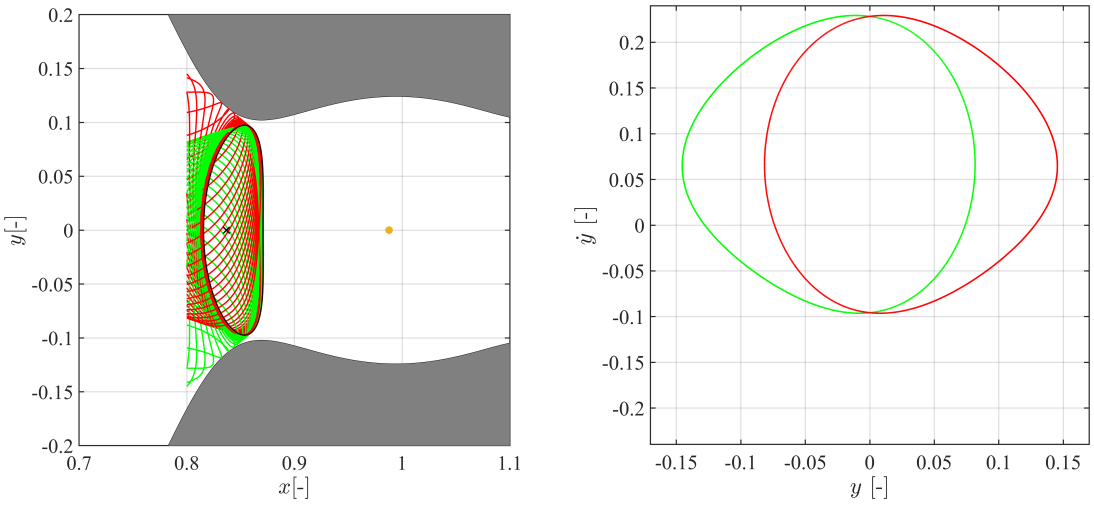

(a) In the x-y plane

(b) Poincaré section at $x = 0.8$

Figure 11: Stable (green) and unstable (red) manifolds of the L_1 Lyapunov orbit in the CR3BP with $C_J = 3.16$

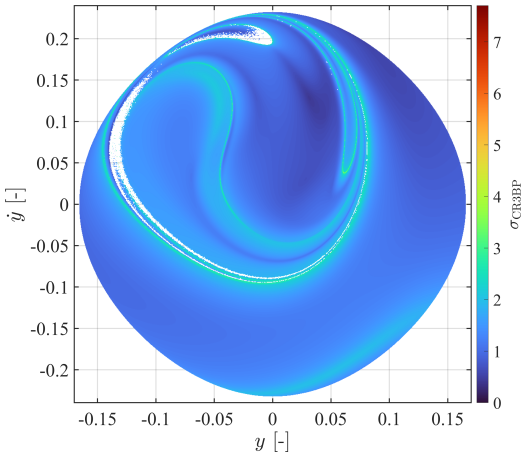

(a) In the CR3BP

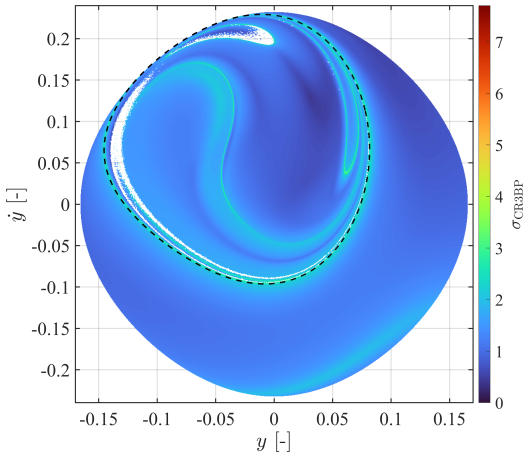

(b) In the CR3BP (with the stable manifold of the L_1 Lyapunov orbit)

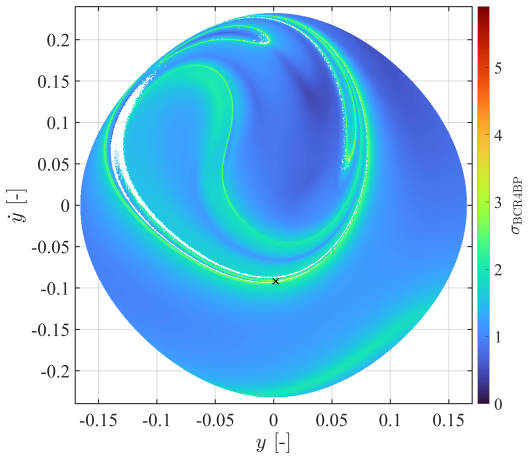

(c) In the BCR4BP (with the optimal trajectory in Figure 9)

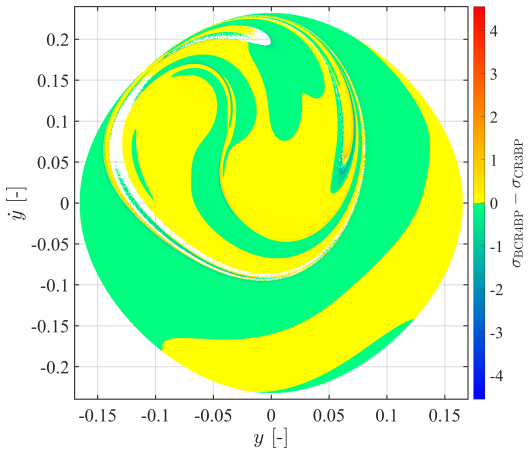

(d) Difference of the FTLE fields in the CR3BP and BCR4BP

Figure 12: Forward-time FTLE fields at $x = 0.8$ in the CR3BP and BCR4BP

Comparison with the literature

The obtained results in the previous section are compared with the results of impulsive interior transfers from the LEO to the LLO in the literature[12–20] based on Reference 13. These results in the literature utilize different dynamical models to design the transfers, so this is not an exact comparison. However, the results in the literature are useful to estimate the Pareto solutions for this optimization and demonstrate the effectiveness of the proposed method. Specifically, Sweetser[12] estimated the theoretical minimum total ΔV (3726 [m/s]) for the transfer between the LEO and LLO. Topputo[13] calculated the Hohmann transfer between these LEO and LLO, which has the total ΔV of 3954 [m/s] and the time of flight of 5 [day]. The result of the comparison is summarized in Figure 13. The obtained result for $\theta_s^* = 0$ is plotted as a red point in the figure. This figure demonstrates that the proposed method can find one of the Pareto solutions with a medium transfer time.

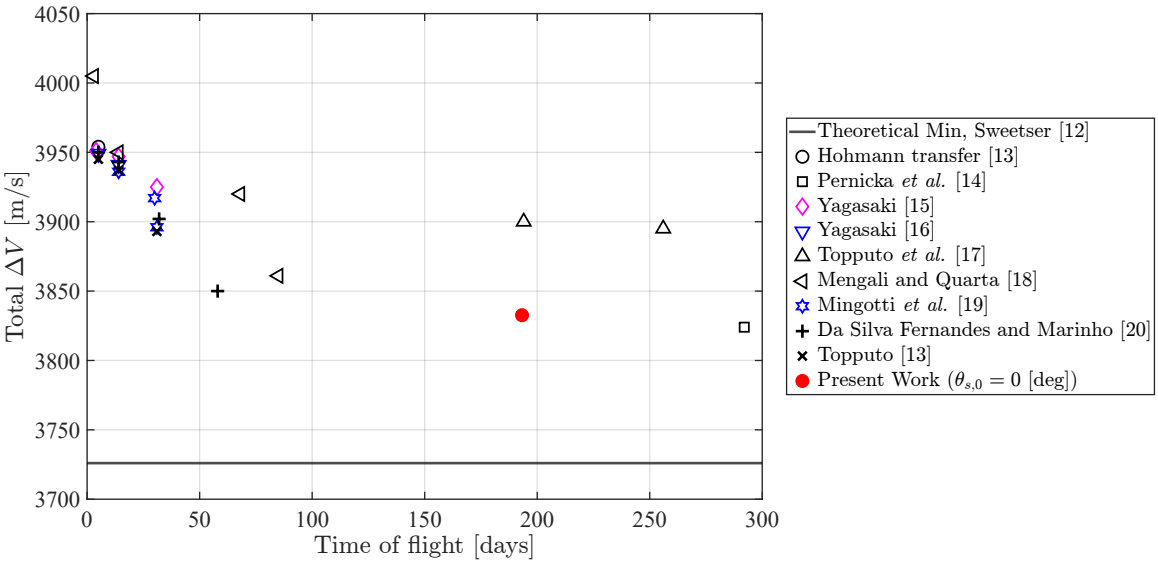

Figure 13: Comparison of the fuel consumption and time of flight

This optimal transfer with $\theta_s^* = 0$ is suitable for the missions strictly limiting the fuel consumption such as the CubeSat missions. Note that it may be possible to find better solutions by adjusting the initial point along the LEO, the final point along the LLO, and the initial phase angle of the Sun.

CONCLUSION

This study applied the trajectory design method based on lobe dynamics to the design of Earth–Moon transfers in the CR3BP and BCR4BP and demonstrated the effectiveness of this method. In the CR3BP, the proposed method enabled to construct fuel-efficient transfers by connecting chaotic trajectories within lobes systematically based on lobe dynamics. The optimal transfer in the CR3BP was then utilized as the initial guess to solve the optimization problem to find the transfers in the BCR4BP. The obtained optimal transfer in the BCR4BP was analyzed by computing the finite-time Lyapunov exponent and detecting the Lagrangian coherent structures. This analysis revealed that this transfer utilizes the region divided by this Lagrangian coherent structure for the transfer to the Moon and this region acts like the stable manifold of the L_1 Lyapunov orbit. The comparison of the fuel consumption and time of flight with the known results in the literature[12–20] demonstrated the effectiveness of the proposed method. Specifically, the proposed method found one of the Pareto optimal transfers between the LEO and LLO, and it was revealed that the obtained transfer in the BCR4BP would be useful especially for the mission under the strict fuel consumption constraint such as the CubeSat missions.

ACKNOWLEDGMENT

The first author thanks the support of Japan Society for the Promotion of Science (JSPS) KAKENHI Grant No. JP 23KJ1692.

REFERENCES

[1] W. S. Koon, M. W. Lo, J. E. Marsden, and S. D. Ross, "Heteroclinic connections between periodic orbits and resonance transitions in celestial mechanics," *Chaos*, Vol. 10, No. 2, 2000, pp. 427–469.

[2] W. S. Koon, M. W. Lo, J. E. Marsden, and S. D. Ross, *Contemporary Mathematics*, Vol. 292, ch. Constructing a Low Energy Transfer Between Jovian Moons, pp. 129–145. American Mathematical Society, Providence, Rhode Island, 2002.

[3] G. Gómez, W. S. Koon, M. W. Lo, J. E. Marsden, J. Masdemont, and S. D. Ross, "Connecting orbits and invariant manifolds in the spatial restricted three-body problem," *Nonlinearity*, Vol. 17, No. 5, 2004, pp. 1571–1606.

[4] S. D. Ross, W. S. Koon, M. W. Lo, and J. E. Marsden, "Application of Dynamical Systems Theory to a Very Low Energy Transfer," *Advances in the Astronautical Sciences*, Vol. 119, 2005, pp. 2991–3004.

[5] B. P. McCarthy and K. C. Howell, "Four-body cislunar quasi-periodic orbits and their application to ballistic lunar transfer design," *Advances in Space Research*, Vol. 71, No. 1, 2023, pp. 556–584.

[6] D. B. Henry and D. J. Scheeres, "Fully numerical computation of heteroclinic connection families in the spatial three-body problem," *Communications in Nonlinear Science and Numerical Simulation*, Vol. 130, 2024, p. 107780.

[7] N. Hiraiwa, M. Bando, I. Nisoli, and Y. Sato, "Designing robust trajectories by lobe dynamics in low-dimensional Hamiltonian systems," *Physical Review Research*, Vol. 6, 2024, L022046.

[8] S. T. Scheuerle Jr., K. C. Howell, and D. C. Davis, "Energy-informed pathways: A fundamental approach to designing ballistic lunar transfers," *Advances in Space Research*, 2024.

[9] V. Rom-Kedar and S. Wiggins, "Transport in Two-Dimensional Maps," *Archive for Rational Mechanics and Analysis*, Vol. 109, 1990, pp. 239–298.

[10] E. M. Bollt and J. D. Meiss, "Targeting chaotic orbits to the Moon through recurrence," *Physics Letters A*, Vol. 204, No. 5, 1995, pp. 373–378.

[11] C. G. Schroer and E. Ott, "Targeting in Hamiltonian systems that have mixed regular/chaotic phase spaces," *Chaos*, Vol. 7, No. 4, 1997, pp. 512–519.

[12] T. H. Sweetser, "An estimate of the global minimum Δv needed for Earth–Moon transfer," *Advances in the Astronautical Sciences*, Vol. 75, 1991, pp. 111–120.

[13] F. Topputo, "On optimal two-impulse Earth–Moon transfers in a four-body model," *Celestial Mechanics and Dynamical Astronomy*, Vol. 117, 2013, pp. 279–313.

[14] H. J. Pernicka, D. P. Scarberry, S. M. Marsh, and T. H. Sweetser, "A search for low Δv Earth–to–Moon trajectories," *Astrodynamics Conference, Scottsdale, AZ, USA*, 1994.

[15] K. Yagasaki, "Computation of low energy Earth–to–Moon transfers with moderate flight time," *Physica D*, Vol. 197, 2004, pp. 313–331.

[16] K. Yagasaki, "Sun-perturbed Earth–to–Moon transfers with low energy and moderate flight time," *Celestial Mechanics and Dynamical Astronomy*, Vol. 90, 2004, pp. 197–212.

[17] F. Topputo, M. Vasile, and F. Bernelli-Zazzera, "Earth–to–Moon Low Energy Transfers Targeting L_1 Hyperbolic Transit Orbits," *Annals of the New York Academy of Sciences*, Vol. 1065, 2005, pp. 55–76.

[18] G. Mengali and A. Quarta, "Optimization of Biimpulsive Trajectories in the Earth–Moon Restricted Three-Body System," *Journal of Guidance, Control, and Dynamics*, Vol. 28, No. 2, 2005, pp. 209–216.

[19] G. Mingotti and F. Topputo, "Ways to the Moon: A Survey," *21th AAS/AIAA Space Flight Mechanics Meeting, New Orleans, LA, USA*, 2011.

[20] S. Da Silva Fernandes and C. M. P. Marinho, "Sun Influence on Two-Impulsive Earth–to–Moon Transfers," *22nd International Symposium on Space Flight Dynamics, Sao José dos Campos, Brazil*, 2011.

[21] V. Rom-Kedar, A. Leonard, and S. Wiggins, "An analytical study of transport, mixing and chaos in an unsteady vortical flow," *Journal of Fluid Mechanics*, Vol. 214, 1990, pp. 347–394.

[22] D. A. Vallado, *Fundamentals of Astrodynamics and Applications*. Microcosm Press, Hawthorne, CA, 4 ed., 2013.

[23] G. Haller and G. Yuan, "Lagrangian coherent structures and mixing in two-dimensional turbulence," *Physica D*, Vol. 147, No. 3, 2000, pp. 352–370.

[24] G. Haller, "Distinguished material surfaces and coherent structures in three-dimensional fluid flows," *Physica D*, Vol. 149, No. 4, 2001, pp. 248–277.

[25] G. Haller, "Lagrangian Coherent Structures," *Annual Review of Fluid Mechanics*, Vol. 47, 2015, pp. 137–162.

[26] C. R. Short, K. C. Howell, and X. M. Tricoche, "Lagrangian Coherent Structures in the Restricted Three-Body Problem," *21st AAS/AIAA Space Flight Mechanics Meeting, New Orleans, LA, USA*, 2011.

[27] D. Pérez, G. Gómez, and J. J. Masdemont, "Detecting Invariant Manifolds Using Hyperbolic Lagrangian Coherent Structures," *1st IAA Conference on Dynamics and Control of Space Systems (DyCoSS), Porto, Portugal*, 2012.

[28] E. S. Gawlik, J. E. Marsden, P. C. Du Toit, and S. Campagnola, "Lagrangian coherent structures in the planar elliptic restricted three-body problem," *Celestial Mechanics and Dynamical Astronomy*, Vol. 103, 2009, pp. 227–249.

[29] C. R. Short and K. C. Howell, "Lagrangian coherent structures in various map representations for application to multi-body gravitational regimes," *Acta Astronautica*, Vol. 94, 2014, pp. 592–607.